Journal Pre-proof

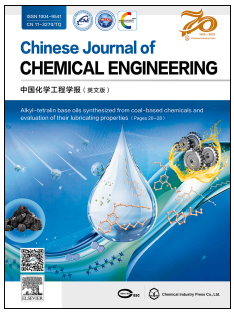

Synthesis of magnesium hydroxide nanoparticles by spontaneous chemical reaction between aerosolized phases at room temperature conditions

Andrea P. Reverberi, Marco Vocciante, Marco Salerno, Omar Soda, Bruno Fabiano

PII: S1004-9541(26)00066-2

DOI: https://doi.org/10.1016/j.cjche.2026.01.010

Reference: CJCHE 3847

To appear in: *Chinese Journal of Chemical Engineering*

Received Date: 18 September 2025

Revised Date: 9 January 2026

Accepted Date: 12 January 2026

Please cite this article as: A.P. Reverberi, M. Vocciante, M. Salerno, O. Soda, B. Fabiano, Synthesis of magnesium hydroxide nanoparticles by spontaneous chemical reaction between aerosolized phases at room temperature conditions, *Chinese Journal of Chemical Engineering*, https://doi.org/10.1016/j.cjche.2026.01.010.

Title:

"Low-temperature synthesis of magnesium hydroxide nanoparticles by spontaneous chemical reaction between aerosolized phases".

Authors and affilaitions;

Andrea P. Reverberi , *DCCI – Department of Chemistry and Industrial Chemistry, Genova University, via Dodecaneso 31, 16146 Genova, Italy*
Andrea.reverberi@unige.it

Marco Vocciante, *DCCI – Department of Chemistry and Industrial Chemistry, Genova University, via Dodecaneso 31, 16146 Genova, Italy*
Marco.voccainte@unige.it

Marco Salerno, *DIFI – Department of Physics, Genoa University, via Dodecaneso 33, 16146 Genoa, Italy*
Marco.salerno@unige.it

Omar Soda, *DCCI – Department of Chemistry and Industrial Chemistry, Genova University, via Dodecaneso 31, 16146 Genova, Italy*
Omar.soda@unige.it

Bruno Fabiano - *DICCA – Department of Civil, Chemical and Environmental Engineering, Polytechnic School, Genova University, via Opera Pia 15, 16145 Genova, Italy*
brown@unige.it corresponding author

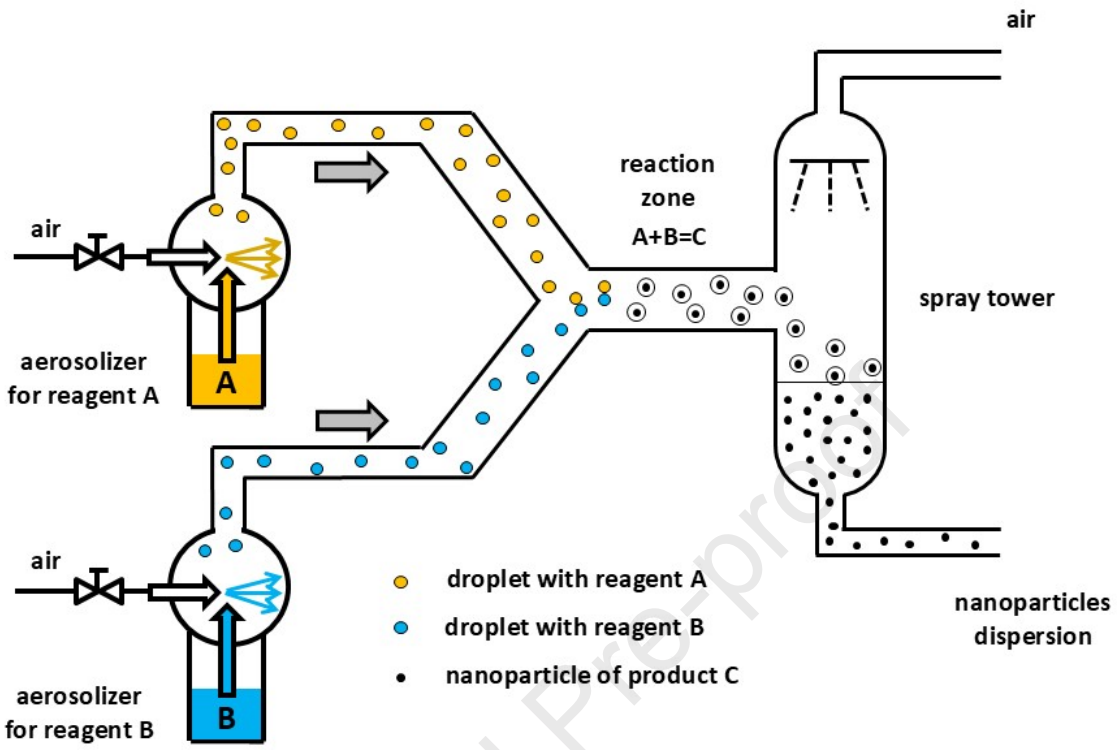

Article

Synthesis of magnesium hydroxide nanoparticles by spontaneous chemical reaction between aerosolized phases at room temperature conditions

A.P. Reverberi[1], M. Vocciante[1], M. Salerno[2], O. Soda[1], B. Fabiano[3]*

[1]*DCCI – Department of Chemistry and Industrial Chemistry, Genoa University, via Dodecaneso 31, 16146 Genoa, Italy*

[2] *DIFI – Department of Physics, Genoa University, via Dodecaneso 33, 16146 Genoa, Italy*

[3]*DICCA – Department of Civil, Chemical and Environmental Engineering, Polytechnic School, Genoa University, via Opera Pia 15, 16145 Genoa, Italy*

*Corresponding author: B. Fabiano (brown@unige.it)

Abstract

A flameless method for the synthesis of nanoparticles at room temperature by coalescence of aerosolized droplets inducing a spontaneous chemical reaction between precursors is presented. The process is tested for the production of magnesium hydroxide nanoparticles at room temperature with an experimental setup based on pneumatic atomizers, condense collectors, mixers and a scrubber separator quenching the process of nanoparticle aggregation and collecting the final product in an aqueous dispersion recycled to the spray tower by a closed pressurized circuit. The solid phase is characterized for shape and composition by field emission scanning electron microscopy and for dimension by dynamic light scattering, with average diameters in a range of 29–62 nm. It has been proven that the quality of the final product depends, in order of decreasing influence, on the volume of the reaction chamber and on the concentration of the reagents in the aerosolized droplets. The process does not require the use of capping agents and/or surfactants aiming at damping particles aggregation and it allows obtaining an uncontaminated product whose composition makes it particularly attractive for specific applications where a high purity is needed, like biochemistry, pharmaceutics and theranostics. The mild operating conditions, the low energy demand and relatively low cost of the required equipment allow including this technique in the context of green, inherent safer and sustainable processes for nanoparticles synthesis.

Keywords: Aerosol, Chemical processes, Inherent safety; Magnesium hydroxide, Nanoparticles, Green technology.

1. Introduction

The methods adopted for inorganic nanoparticles (NPs) synthesis rely upon a wide variety of processes, generally carried out in liquid phase for different reasons, including an easy control of the final product and its spatial confinement [1]. Very often, these techniques are implemented only on a laboratory scale, namely they are limited to a research area rather than transferred to a well-established industrial production. The methods adopted for NPs synthesis are generally based on a combination of chemical and physical process whose energy transfer is based on thermal dissociation [2], electromagnetic radiation, cold plasma and on differences in electrochemical and redox reactions [3]. The latter are particularly important in bottom-up metal NPs synthesis, a technique that frequently implies hazardous reagents characterized by inherent toxic, corrosive and/or flammable properties [4]. Well-known examples include zerovalent NPs synthesis in aqueous solvents, where reducing agents such as sodium borohydride or hydrazonium compounds are used [5].

Reverse-micelle and emulsion methods [6] merit an extra mention, as they rely upon a mechanism of local spatial confinement of reaction volumes, actually making the synthesis occur in a segregated ensemble of microreactors having the dimension of a single micelle, thus damping the aggregation between different reaction domains [7]. Likewise, biological processes are successfully developing [8], thanks to their environmental soundness and economicity [9] and recently woody biomass-derived organosolv lignin nanoparticles were synthesized via a simple and facile anti-solvent nanoprecipitation technique and used for the fabrication of ultrafiltration nanocomposite membrane [10].

Aerosol-based processes for NPs synthesis belong to a field more closely related to large-scale production and they include aerosolized flame processes [11], flameless thermal dissociation of aerosolized precursors, plasma/laser synthesis and chemical synthesis by mechanically/electrically driven coalescence, as indicated in the scheme reported in Fig. 1.

In vapor-aerosol flame synthesis (VAFS), a gas stream carrying a precursor in gaseous state or in fine liquid droplets is fed at the inlet of a burner together with gaseous combustible and comburent streams [12]. A high temperature produced by a flame front triggers a pyrolysis of the precursor with formation of nanosized powders [13]. Basic parameters of this technique are the flame temperature, the combustion regime with its fluid dynamics, the residence time inside the burner and the matching of the following flame quenching by which the particle size growth is finally stopped [14]. This process, initially focused on the production of carbon black, is nowadays a cornerstone for the industrial synthesis of inorganic nanopowders having great thermal stability, like SiO_2 [15], TiO_2 [16], Al_2O_3 [17] and SnO_2 [18]. Additionally, the use of reducing flames in aerosolized flame NPs synthesis proved to be suitable for the preparation of metal NPs thanks to a beneficial effect in damping the surface oxidation for the realization of carbon–metal and metal–ceramic nanocomposites.

The flameless thermal dissociation of precursors contained in aerosols is essentially based on two consecutive stages [19]. In the former, a precursor dispersed in a solvent is aerosolized in a gas stream. In the

latter, the precursors are subject to a chemical dissociation together with other physical processes, like solvent evaporation, leading to the formation of the relevant NPs. A typical example of this technique is spray pyrolysis, where the NPs synthesis may occur even in the absence of solvents, as in the production of zerovalent Ni NPs and nanowires from thermal dissociation of the corresponding carbonyl $Ni(CO)_4$, previously dispersed in a gaseous stream [20]. In the production of molecular sieves, a precursor made of a mixture of organo-metallic compounds containing Si and Ti is nebulized and further dried in a quartz tube at 200 °C [21].

In plasma- or laser-assisted synthesis processes, a ionized gas stream acts on a precursor dispersed in droplets, thus determining a chemical reaction in the precursor triggering a NPs synthesis, followed by a gas quenching to stop a further particle aggregation. In thermal plasmas, where the electrons are in thermal equilibrium with nuclei, the aerosolized precursor undergoes dissociation by means of an electric arc, as in plasma spray synthesis (PSS), generally carried out by suitable nozzles equipped with an arc discharge chamber. With this technique, refractory powders and even metal NPs have been obtained, thanks to its versatility and its possibility of using inert gases as carriers, thus damping metal oxidation. In cold plasma synthesis, an electrical discharge at high voltage and low current intensity is used. An example is surface dielectric barrier discharge processes (SDBD), where an aerosolized precursor crosses an array of silent discharge electrodes. Good temperature control allows obtaining organic NPs hindering their thermolysis [22].

In chemical synthesis by mechanically/electrically driven coalescence, droplets containing precursors are formed by electrodynamic or pneumatic atomization of liquid phases whose further coalescence is induced by mechanical action or by the presence of an electric field, producing a mixing and a chemical reaction leading to NPs formation [23]. A variant of this technique, based on a reaction between an aerosolized phase and a liquid, proved to be advantageous to realize monodisperse Au NPs at mild operating conditions [24].

Except for the last synthesis technique, all other methods imply demanding operative conditions in terms of energy consumption, process and occupational risk and environmental impact.

As recently highlighted, the preferred order of consideration of risk-reduction measures (ranking from most to least effective) is inherently safer design (ISD), passive engineered, active engineered and management [25]. Consequently, in order to overcome the above-mentioned limitations, technological innovation in the production process should follow the Inherent Safety Design (ISD) concepts, introducing intrinsic changes at the process conceptualization phase by a quantitative comparison of different conceptual design solutions [26] to eliminate the hazards, or dramatically reduce their impact, thus obtaining more reliable and easier to operate plants. Even though this approach dates back to the Eighties, currently it represents common sense in the process sector, while its adoption is not common practice in NPs production plants. Process design evidencing the attainment of lower hazards and lower requirements for providing layers of protection were proposed only in the last years [27].

The present study is in line with ISD broad framework, as it proposes a NPs synthesis process at room temperature based on a spontaneous chemical reaction between pneumatically aerosolized phases, each of them containing a precursor, whose droplets are made to coalesce at atmospheric pressure by simple mixing in the absence of a force field imposed by an external operator, using air as carrier gas. The NPs are collected in a liquid phase by crossing a countercurrent spray curtain produced by a sequence of nozzles located in a scrubber. Notably, the here-presented process and plant operate at attenuated conditions in terms of T and P, avoid the use of hazardous auxiliaries and solvents for the synthesis and minimize the reaction steps as well. These tricks allow circumventing the drawbacks related to a multistep process and derivatization, generally connected with an intensive use of chemical reagents which often decrease the overall atomic efficiency of the process [28].

This process, differing from previous ultrasonic aerosol-assisted synthesis methods [29], has been tested in the synthesis of $Mg(OH)_2$ NPs, owing to its easy formation at room temperature and its very low toxicity. This compound proved to be an efficient flame retardant [30], a nanosorbent for environmental decontamination [31], an effective storage material [32], a nanocarrier for drug delivery [33] and a nanofiller for bone scaffolds [34]. $Mg(OH)_2$ may act as a valid substrate in the photocatalytic water splitting for the production of hydrogen by visible light [35], thus representing an economically appealing alternative to other emerging photocatalytic techniques [36]. Moreover, $Mg(OH)_2$ can be considered as a source material for the preparation of nanosized MgO and its composites, having good performances in heavy metal removal [37], removal of fluoride from wastewater when loaded on the surface of aeolian sand [38], in CO_2 capture [39] and in low-temperature catalytic conversion of CO [40].

A very exhaustive discussion on the synthesis and application of nanostructured $Mg(OH)_2$ can be found in the review paper of Balducci *et al*. [41].

In the proposed process, the only required energy contributions are those pertaining to the aerosol formation and to the scrubber functioning, thanks to a synthesis carried out at room temperature. This is one of the main aspects making the difference between the present technique and the other aerosol-based methods reported in past literature. The remainder of the paper is divided as follows. In section 2, the experimental apparatus is described together with all the relevant operating conditions. In Section 3, the results are discussed, and the NPs are characterized according to the techniques described in the previous section. In Section 4, the main research challenges are outlined and conclusions are drawn in view of future applications of the designed process.

AEROSOL-BASED TECHNIQUES FOR NANOPARTICLES SYNTHESIS	
PHYSICO-CHEMICAL METHODS	**Aerosolized-flame processes** (flame aerosol technology; flame spray synthesis)
	Flameless thermal dissociation of aerosolized precursors (spray pyrolysis; chemical aerosol flow synthesis; solution aerosol thermolysis)
	Plasma/laser synthesis (aerosol through plasma method ATP; plasma spray synthesis PSS; surface dielectric barrier discharge SDBD)
	Chemical synthesis by electrically-driven coalescence (electrospraying with reaction; bipolar mixing)
	Chemical synthesis by mechanically-driven coalescence (vibrating nozzles)
PHYSICAL METHODS	**Spray drying**
	Electrospraying without chemical reaction

Fig. 1. Scheme of different aerosol techniques adopted in NPs synthesis.

2. Materials, methods and experimental setup

2.1. Chemicals

Magnesium sulfate ($MgSO_4$, 99.5%, Sigma-Aldrich, Milano, Italy), sodium hydroxide (NaOH, 99%, La Farmochimica, Genova, Italy) have been used as purchased. In the experimental campaign here adopted, these chemicals have been dissolved in bidistilled water at concentrations of 0.01 and 0.02 $mol \cdot L^{-1}$ for $MgSO_4$ and 0.02, 0.04 for NaOH, in order to match the stoichiometry of the following reaction:

$$MgSO_4 + 2NaOH \rightarrow Mg(OH)_2 + Na_2SO_4 \quad (1)$$

An equal volume of each solution is poured in the corresponding pneumatic aerosolizer (one for $MgSO_4$ solution and the other for NaOH solution). These devices will be described in section 2.3. In the following, the precursors $MgSO_4$ and NaOH will be named with letters A and B, while the products C and D represent the nanosized water-insoluble solid phase made of $Mg(OH)_2$ NPs and the water-soluble Na_2SO_4 salt produced by Eq. (1).

2.2. Characterization techniques

Particle diameters have been determined by dynamic light scattering (DLS). To this purpose, a Zetasizer Nano ZS (Malvern Instruments, UK) was used in size measurement mode. A PMMA cuvette, with suitable flat and smooth walls, was employed as reservoir for each sample of liquid, approximately 1.2 ml volume. The optical transparency of the cuvette walls ensures the transmission of the red laser light. Bidistilled water was used as embedding liquid to adjust the dilution of the sample at 20 °C, while the values of the refractive index and of the absorption coefficient for $Mg(OH)_2$ were fixed at 1.56 and 0.01, respectively. Six different

measurements allowed to determine the time autocorrelation function of the scattered light with the purpose of finding the particle size distribution by intensity as the raw data. The size distribution by volume and by number were automatically obtained within the instrument software after specific modeling. The measurements were repeated in case of data instability and a final data regression allowed obtaining the corresponding representative curves in scatter graph, subsequently fitted with lognormal distribution.

A Carl Zeiss AG - SUPRA 40VP (Germany) instrument was adopted to carry out the field emission scanning electron microscopy (FESEM) analysis of the particles. A sample of the liquid (20 µl) containing the NPs was deposited on a polymeric filter (Isopore membrane filter, with 200 nm pore diameter), to determine the particle morphology. A liquid sample was repeatedly deposited and further dried for six times, aiming at obtaining sufficient particle concentration on the substrate. After a final drying phase lasting 12 h, the filter was located on an aluminum holder and sputter coated with a graphite film for the purpose of increasing the electrical conductivity of the sample. FESEM analyses were carried out with an accelerating voltage of 10 kV and a maximum magnification of 500'000X. The instrument is equipped with a Pentafet Si(Li) detector for energy dispersive X-ray spectroscopy (X-EDS). The EDS spectrum was collected for 60 s with a primary beam energy of 10 keV and a probe current of 230 pA.

X-ray powder diffraction analysis (XRPD) was carried out by a vertical diffractometer X'Pert MPD (Philips, Almelo, the Netherlands), equipped with a Cu tube (Kα1 wavelength: 0.154 nm). The samples were comminuted in an agate mortar and the patterns were collected in a 2θ range between 10° and 100°, with a step of 0.001° and measuring time of 50 s/step. The indexing of the obtained diffraction data was performed in comparison with literature data.

2.3. Experimental setup

In Fig. 2, two different choices of pneumatic nebulizers, typically used in medical aerosol therapy are presented. Both of them operate according to the principle of the Venturi nozzle, in which a liquid is aspirated and atomized by a depression caused by an increase of the carrier gas velocity. The left image of Fig. 2 refers to a DeVilbiss nebulizer of traditional design, with a glass ampoule having a maximum liquid volume capacity of 5 cm^3 and an inner air orifice of 0.6 mm. A plastic-made nebulizer, as the Updraft nebulizer visible in the right image of the same figure, offers the advantage of having an internal chamber that can be inspected, but after an initial attempt to use it, it was essentially discarded for safety reasons, due to its imperfect seal, which makes it unsafe in the case of highly alkaline solutions, whose aerosols may be very aggressive to the respiratory system. Hence, for the present experimental campaign, where a NaOH solution is used as precursor, a glass-made atomizer seemed to be the most preferable choice, which was adopted in all tests, carried out at room temperature. More sophisticated techniques of aerosols generation with higher efficiency and narrower droplet size distribution were proposed in scientific literature [42], but the present choice may represent a trade-off between cost-effectiveness and technical performance.

Upstream of each atomizer, a rotameter and an analogic pressure gauge ensure a suitable air feed control, whose flow rate is equally distributed between both atomizers to avoid an excess of a single precursor. This process facet will be thoroughly reconsidered in the following section.

Each atomizer is equipped with a perforated silicone cap with a glass fitting, which conveys the nebulized stream towards a condense separator, in order to collect the liquid film resulting from coalescence of part of the sprayed droplets on the walls of the pipes. This is an empty, round-end cylindrical glass container with a volume of 50 cm^3, at the bottom of which a liquid film is collected to prevent it from reaching the reaction zone. Afterwards, both aerosolized streams enter the reaction zone, where they are merged together leading to a coalescence between droplets giving rise to a spontaneous chemical reaction described by Eq. (1).

Fig. 2. Images of two different pneumatic nebulizers commercially adopted in pharmacotherapy: a DeVilbiss glass nebulizer (a) and an Updraft plastic nebulizer (b).

This reaction zone has been realized according to three different plant solutions that have been reported in Fig. 3. The scheme (a) refers to a cylindrical mixing-reaction chamber of 140 cm^3 volume. The schemes (b) and (c) refer to a simple "Y" and "T" shaped connector, where the aerosolized streams are mixed together, replacing the mixing chamber of scheme (a). Both mixers and tubes employed in this experimental setup have an inner diameter of 7 mm. The length of the tube downstream the reaction zone (0.5 m) is the same for all three cases and is characterized by a volume of 19.24 cm^3. The effects of different connectors which merge together the aerosolized streams may dramatically influence the quality of the final product and this aspect will be reconsidered in the following section. The coalescence between droplets coming from different streams (and each containing the respective precursor A and B) produces $Mg(OH)_2$ NPs as a water-insoluble product C embedded in a water droplet, containing also the water-soluble reaction product D.

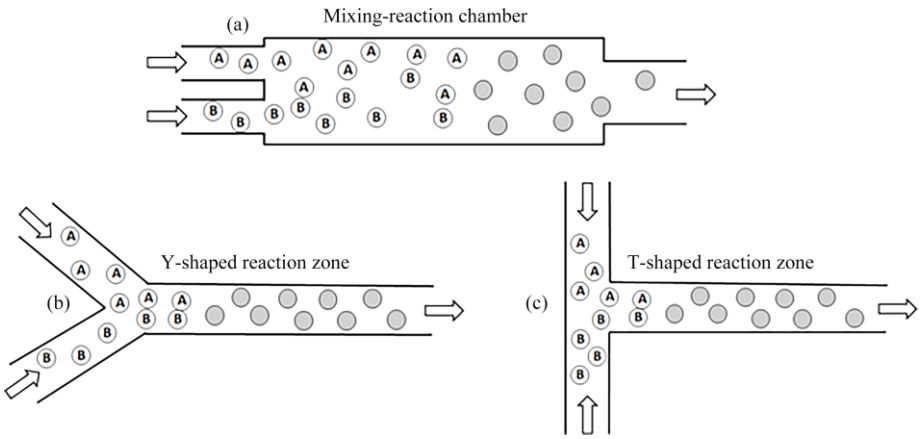

Fig. 3. Scheme of the mixing-reaction zone, according to three different set-up configurations. The upper panel (a) refers to a mixing chamber where the droplets have a high average residence time, with a greater probability of homogeneous coalescence between droplets containing the same precursor, leading to an increase of microreactor volumes. The lower panels (b) and (c) refer to a Y-shaped and a T-shaped mixer ideally without axial mixing, thus minimizing NPs agglomeration. A and B are the precursors, while grey discs represent the coalesced droplets. All devices operate horizontally.

The stream leaving the reaction zone, carrying both coalesced and non-coalesced droplets, enters a spray tower of cylindrical shape from below in a tangential direction to its lateral surface through a semicircular inflow duct, giving a helical rising trajectory to the droplets containing the NPs. During their rising motion, the droplets collide with full-cone liquid sprays of water produced by four atomizing nozzles located at different heights along the scrubber axis. The spray cone angle is larger enough to reach the lateral surface of the separator, thereby producing a liquid falling film dripping on the tower bottom, where it forms a liquid layer of constant level, embedding the NPs of the product C and the dissolved compound D. In turn, this liquid is sucked out by a peristaltic pump and further transferred to the four aforementioned nozzles, thus realizing a close circuit of liquid which is progressively enriched of NPs for growing time. The two-rollers peristaltic pump (Espango, mod. IPS200) is equipped with a 24 V/50 W DC motor connected to an adjustable power supply, giving a maximum allowed pressure of 200 kPa at the nozzles.

The air stream comes out of the scrubber by flowing through a special trap of glass beads located at its top and collecting the droplets that have not been entrapped by the sprays, as a first step of their abatement.

Subsequently, the air is conveyed to a sequence of bubblers as traps aiming at capturing the remaining droplets and NPs to avoid their venting in the atmosphere.

It should be noted that the scrubber does not work only like a simple droplet/NPs collector. In fact, it has an even more important function of reaction-quenching as a secondary effect of droplets dilution in a relatively large mass of liquid. During the working cycle, an aliquot of liquid can be spilled from the bottom of the scrubber to perform the necessary analysis and characterization of the NPs. The overall layout of the setup is reported in Fig. 4.

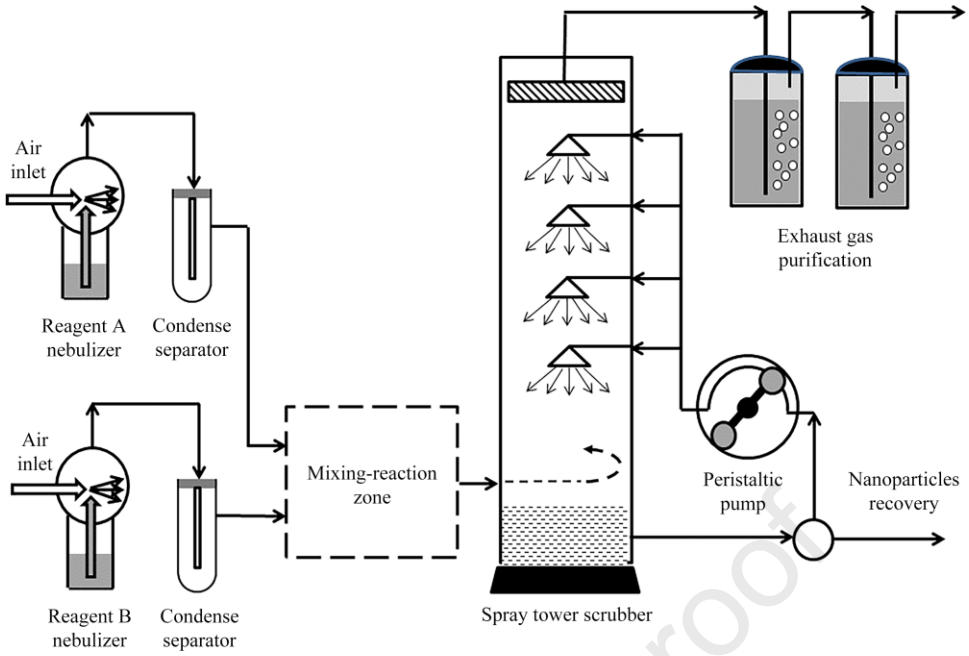

Fig. 4. Schematic layout of the plant. The mixing-reaction zone has been described in detail in Fig. 3.

3. Results and Discussion

The aforementioned experimental setup operates in a continuous mode as far as the droplet reactor is concerned, owing to its intrinsic configuration, typical of an open system. However, the atomizers operate in batch mode, as they stop functioning when the liquid contained in them has been totally aerosolized. In fact, the atomizers may hold a limited liquid volume, as indicated in subsection 2.3, and this constraint makes it necessary to stop the unit running to refill them. In Fig. 5(a), a scatter plot of the aerosolized mass versus the inlet air pressure is reported for a single nebulizer. As expected, irrespective of precursor species, the mass of droplets conveyed in the air stream is proportional to the inlet pressure p, but a threshold value p_0=40 kPa exists, below which the device runs irregularly with fluctuations in droplets generation, as it operates in conditions far from its nominal settings. On the other hand, high values of inlet pressure are not beneficial, as they imply a growing air flow rate which may reduce the efficiency of the scrubber with an unwanted product loss. For the aforementioned reasons, all experiments were carried out at an inlet pressure of 40 kPa for each aerosolizer. In Fig. 5(b), the inlet gas flow rate is plotted versus the inlet gas pressure. The data are the same for both aerosolizers. Analogous trend has been found in the paper of Li *et al.* [43], where a linear trend between these variables has been reported for air-blast nebulizers.

The process here adopted is based on an operating principle analogous to that typical of the well-known reverse micelle method for the synthesis of nanoparticles in liquid microemulsions. In fact, both techniques rely upon the effect of a reaction confinement in limited volumes, just acting as single isolated microreactors, embedding the NPs during their chemical synthesis occurring by droplet coalescence. Several studies have

been proposed for modelling reaction kinetics by microemulsions in batch processes. Ramesh Kumar *et al*. [44] proposed an analytical method describing the time trend of micelle diameters by means of a set of population balance equations [45], under the assumption of instantaneous chemical kinetics and Brownian regime of micelle collision. Other authors [46] modelled particle growth under the assumption of a diffusion-limited process by which the reactants are fed to the micelles embedding the growing NPs. Monte Carlo models [47] with their variants [48] represent an alternative to the aforementioned analytical approaches and they allow overcoming some computational difficulties typical of a continuum scheme [49], at a price of an extended computation time.

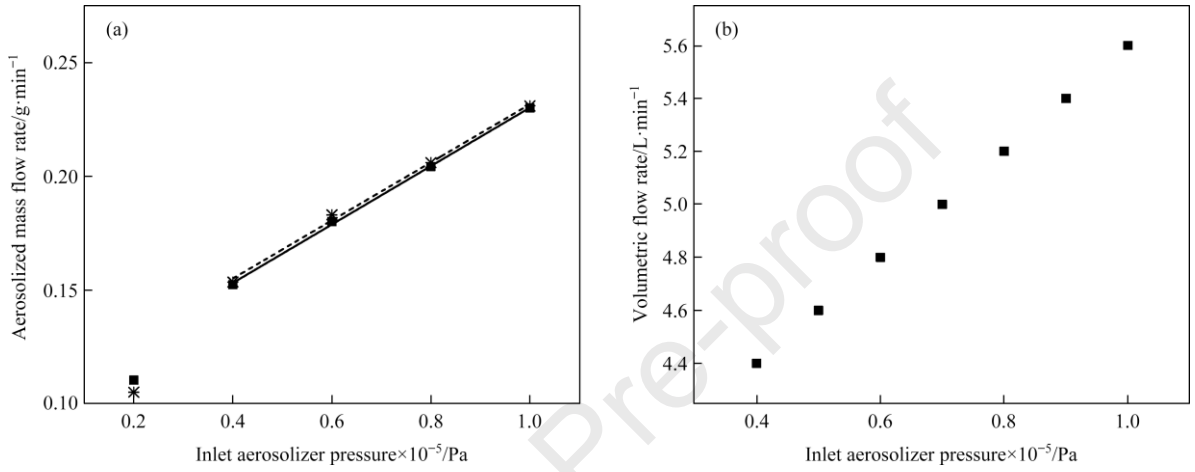

Fig. 5. (a) Plot of the aerosolized mass flow rate versus air feed pressure of each aerosolizer. Solid squares and asterisks refer to 0.2 mol·L^{-1} NaOH and 0.1 mol·L^{-1} $MgSO_4$ solutions. (b) Plot of volumetric inlet gas flow rate versus air feed pressure for each aerosolizer. The data of plot (b) are independent of precursor species or concentration.

Despite the outlined similarity between microemulsion methods and the present technique in terms of reaction volume confinement, it is worth highlighting some peculiar aspects in which the two methods differ in substance, namely:

- In reverse micelle methods, a NPs synthesis occurs by chemical reaction between precursors contained in droplets embedded in a liquid phase. Here, instead, the NPs synthesis is carried out by chemical reaction between precursors contained in droplets embedded in a gaseous phase.
- Surfactants and/or capping agents are constantly present in reverse micelle methods [50] and they allow the stability of emulsions before mixing [51]. However, the separation of the as-formed NPs from the stabilizing agents is not a simple task, often needing complex and expensive unit operations following the synthesis stage, usually requiring the use of noxious solvents endangering the eco-friendliness of the global process.
- A NP chemical synthesis by the reverse micelles technique generally takes place in a closed system, namely in a batch chemical reactor. This is confirmed by all the previously quoted studies here reported as examples of microemulsion NPs synthesis. On the other hand, theoretical and experimental investigations about kinetics of NPs formation by reverse micelles in open systems are

quite uncommon, probably owing to intrinsic difficulties related both to mathematical modelling and to satisfactory process control. Of course, droplet-based microreactors for nanomaterial production in liquid phases are well known and may operate both in batch and in a steady-state regime, but they need a very accurate tuning of the microfluidic conditions for a single droplet manipulation and an accurate choice of microchannels materials ensuring tailored physicochemical characteristics like wettability. The reader is addressed to the recent paper by Liu *et al*. [52] representing an excellent review on this topic.

3.1. Some considerations about different reaction schemes

In case of reactions carried out in open systems where aerosolized droplets spontaneously react by coalescence, as for the schemes reported in Fig. 3, an important descriptor is the residence time distribution (RTD) function of droplets containing the precursors. In order to better understand the effect of different configurations of mixing and reaction zones, it is worth recalling some theoretical aspects pertaining to the RTD of ideal reactors, like the continuous stirred tank (CSTR) and the plug flow reactor (PFR). For a CSTR, the well-known RTD expression assumes the form:

$$f(t) = \frac{1}{\tau_1} e^{-t/\tau_1} \tag{2}$$

where τ_1 is the average residence time in the tank. Eq. (2) represents the typical "broad" configuration of RTD, as all residence times are allowed in the range (0, +∞), though with monotonically decreasing probability.

For a PFR, the situation is completely opposite to the previous one, as the relevant RTD can be written as:

$$f(t) = \delta(t - \tau_2) \tag{3}$$

where $\delta(t-\tau_2)$ is the Dirac delta function centered in the corresponding PFR average residence time τ_2. Hence, Eq. (3) is the "narrowest" possible RTD for a chemical reactor, where only one residence time is allowed.

Applying the above considerations to the cases considered in the present study, one can observe that the scheme reported in Fig. 3(a) consists of a mixing-reaction zone acting as a CSTR, followed by a tubular duct where the droplets carrying the precursors continue to mix and react together like in a PFR. For these reasons, the resulting RTD ideally consistent with the scheme of Fig. 3(a) is that typical of a CSTR and PFR in series, that is:

$$f_{\mathrm{a}}(t)=\begin{cases}\dfrac{1}{\tau_1}e^{-\frac{t-\tau_2}{\tau_1}} & t\geq\tau_2\\ 0 & t<\tau_2\end{cases}$$

(4)

where τ_1 and τ_2 are the residence times of the aerosol droplets in the mixing-reaction chamber and in the downstream tube, respectively.

The RTDs for the schemes of Y- and T-shaped reactors of Fig. 3(b) and (c) are equal and they are those reported in Eq. (3), namely:

$$f_{\mathrm{b,c}}(t)=\delta(t-\tau_2)$$

(5)

The total average residence times τ_{a} and $\tau_{\mathrm{b,c}}$ for all the schemes reported in Fig. 3 can be deduced from Eqs. (4) and (5), namely:

$$\tau_{\mathrm{a}}=\int_0^\infty t\, f_{\mathrm{a}}(t)\mathrm{d}t=\tau_1+\tau_2$$

(6)

$$\tau_{\mathrm{b,c}}=\int_0^\infty t\, f_{\mathrm{b,c}}(t)\mathrm{d}t=\tau_2$$

(7)

Finally, the variances of the corresponding RTD can be determined according to the following expressions:

$$\sigma_{\mathrm{a}}^2=\int_0^\infty (t-\tau_{\mathrm{a}})^2\, f_{\mathrm{a}}(t)\mathrm{d}t=\frac{1}{\tau_1}\int_{\tau_2}^\infty (t-\tau_{\mathrm{a}})^2 e^{-\frac{t-\tau_2}{\tau_1}}\,\mathrm{d}t=\tau_1^2$$

(8)

$$\sigma_{\mathrm{b,c}}^2=\int_0^\infty (t-\tau_2)^2\delta(t-\tau_2)\,\mathrm{d}t=0$$

(9)

The results of the aforementioned considerations have been summarized in Table 1.

Table 1. Statistical properties of RTD according to the different mixing-reaction configurations described in Fig. 3.

Mixing-reaction configuration of Fig. 3	Average residence time (ideal case)	Variance (ideal case)
Case (a): Mixing chamber + downstream tube (CSTR + PFR)	$\tau_1 + \tau_2$	τ_1^2
Case (b): Y-shaped mixer + downstream tube (PFR)	τ_2	0
Case (c): T-shaped mixer + downstream tube (PFR)	τ_2	0

When both aerosolizers operate at an inlet pressure of 40 kPa, the gas flow rate at the exit of each aerosolizer, under the effect of head losses due to the downstream scrubber, is 5.6 $L \cdot min^{-1}$. Under this operative condition, $\tau_1 = 0.75$ s and $\tau_2 = 0.103$ s.

As anticipated in the previous section, in a first experimental campaign, the mixing between the two aerosolized streams, each containing the precursors A and B, has been realized in a mixing-reaction chamber, as depicted in the panel (a) of Fig. 3. However, in accordance with the above presented theoretical insights, the particles of product C obtained with this solution had average diameters >100 nm, namely no longer classifiable as NPs according to the standards adopted by the scientific community [53]. For this reason, the mixing/reaction configuration of Fig. 3(a) has been discarded and the results reported in the following will refer only to the schemes (b) and (c) of Fig. 3, corresponding, under an ideal case of modelling, to a shorter residence time and null variance, as reported in Table 1. Admittedly, an increase in average and dispersion of RTD in the reaction zone did not prove to be beneficial, probably owing to a combination of different effects, namely:

- In the mixing chamber, acting as a CSTR, the streams do not enter in a premixed state, while they enter premixed into the pipe downstream the T- or Y-shaped mixers. This fact motivates, at least qualitatively, a higher probability of homogeneous coalescence, namely a coalescence between droplets belonging to the same stream and containing the same precursor, in the former case.
- Higher τ and σ^2 values, in case of a non-premixed CSTR, may increase the probability of homogeneous coalescence. This phenomenon leads to the formation of droplets of larger diameters, whose further heterogeneous coalescence (between droplets with different precursors) triggers the formation of larger particles of the product C.
- Analogously, higher τ and σ^2 values, in case of a non-premixed CSTR, may enhance the probability of coalescence between droplets where the precursors have already reacted, namely already containing NPs of C, thus increasing the probability of aggregation between NPs of the product C.

These unwanted side-effects are visually represented in the upper panel (a) of Fig. 6. A homogeneous coalescence, statistically more probable in the mixing chamber of Fig. 3(a), acting as a CSTR, may result in larger reaction volumes, with formation of many nucleation seeds inside coalesced droplets, eventually giving particles of bigger diameter by aggregation. Globally, the reaction scheme of Fig. 3(a) relies upon

mechanisms described both in the upper (a) and in the lower (b) panel of Fig. 6, while the reaction scheme of Fig. 3(b) and (c) are preferentially based on mechanism described in the lower panel (b) of Fig. 6.

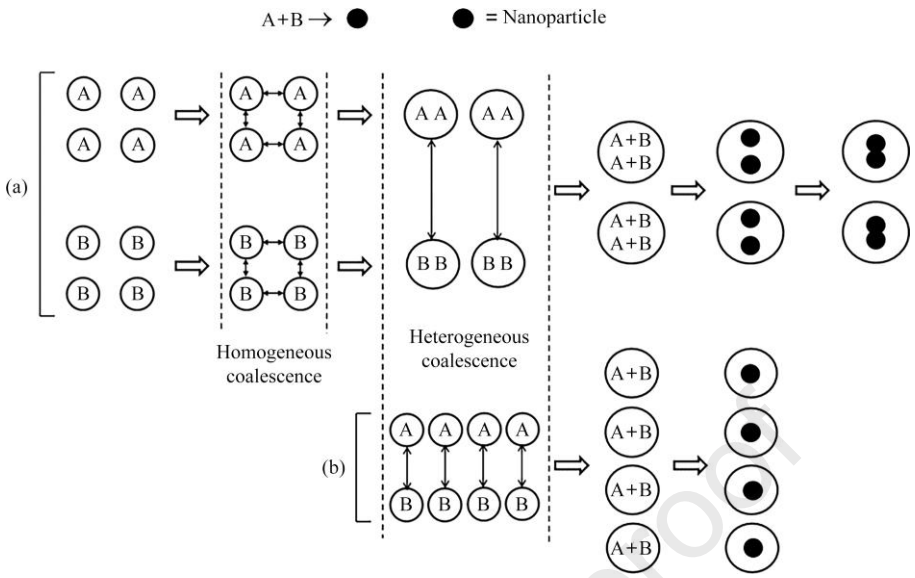

Fig. 6. Scheme of two different synthesis mechanisms. The upper panel (a) represents a reaction by heterogeneous coalescence following homogeneous coalescence, while the lower panel (b) represents a reaction resulting solely from heterogeneous coalescence not preceded by homogeneous coalescence.

As further consideration, it has been observed that that the coalescence between droplets coming from the same nebulizer, namely between droplets containing the same precursor, may also occur upstream the reaction zone. For this reason, the volume of condense separators, reaction zone and pipes have been kept at the minimum possible.

3.2. Some considerations about regimes downstream the mixing zone in case of T- and Y- shaped mixers

Air-blast nebulizers, including the DeVilbiss glass type adopted in this study, represent the most traditional devices used in pharmacotherapy. According to Chen *et al*. [54], these aerosolizers produce droplets having diameters d_p in a range 1–10 μm, with standard deviation of 1.4–2.5 μm. In the absence of specific measurements concerning the diameters of the aerosolized droplets, these diameters values have been adopted to calculate the range of variability of the following dimensionless numbers characterizing the regime of the mixed aerosol streams, in order to motivate the phenomena of droplet coagulation, $Mg(OH)_2$ nucleation and aggregation following coalescence.

The measured gas flow rate Q downstream the T- or Y- shaped mixers for an inlet nebulizer pressure of 40 kPa was 1.866×10^{-4} $m^3\cdot s^{-1}$ for all experimental runs. This gas flow rate is significantly higher than twice the value measured at the nebulisers inlet, due to the variation in the specific volume of the gas upstream and downstream of the nebulisers.

The gas-phase Reynolds number (*Re*) is defined as:

$$Re = \frac{2Q\rho_g}{\pi a \mu}$$

(10)

where ρ_g , μ, and a are the density of the gas, its viscosity and the radius of the tube downstream the mixers. The calculated value *Re*= 2255 for all experiments after mixing the two aerosolized phases, indicates the onset of incipient turbulence.

The Knudsen number (*Kn*) is defined as:

$$Kn = \frac{2\lambda}{d_p}$$

(11)

where λ is the mean free path in air, assumed here to be λ=6.54×10^{-8} m [55].
The Stokes number (*Stk*) is defined as [56]:

$$Stk = \frac{C_c \rho_p d_p^2 Q}{18\pi\mu a^3}$$

(12)

where ρ_p = 1015 kg·m^{-3} is the droplet density, here assumed as an average between the density values corresponding to the different concentration of precursors, whose values do not significantly affect the density of the droplet. C_c is the Cunningham correction factor to the Stokes–Einstein diffusivity, depending on *Kn* according to Heim *et al*. [57]:

$$C_c(Kn) = 1 + Kn\left[1.257 + 0.4\exp\left(\frac{-1.1}{Kn}\right)\right]$$

(13)

Davies [58] pointed out that the aforementioned expression is valid provided *Kn*<15. The present experiments satisfy this constraint.
The Péclet number (*Pe*) can be written as:

$$Pe = Re\,\frac{\mu}{D\rho_g}$$

(14)

D, the particle diffusion coefficient, assumes the form:

$$D = \frac{k_B T C_c}{3\pi\mu d_p}$$

(15)

where k_B is the Boltzmann constant and T is the temperature. The values of the aforementioned dimensionless numbers, for the reference droplet diameter range, excluding *Re*, are reported in Table 2. The values of $Kn \ll 1$ are consistent with a hydrodynamic regime, where the gas can be considered as a continuum [59], bordering a transition regime for $0.1 < Kn < 10$ [60].

The *Stk* range, at least for its highest values close to the unity, is consistent with the onset of coalescence following the merging between aerosolized streams, owing to inertial effects. Additionally, it can explain a non-negligible probability of droplet collisions against the tube walls.

The values of the Péclet number, namely $Pe \gg 1$, suggest that molecular diffusion is negligible, the coagulation is bulk-driven and the tube downstream the mixers, irrespective of their type, can be considered as an ideal PFR, thus motivating the reasoning behind Table 1.

In NPs synthesis according to the scheme described by Eq. (1), a matching between the residence time and the kinetics of supersaturation following coalescence is a basic aspect determining the characteristics of $Mg(OH)_2$ NPs [61]. On that note, according to Yuan *et al*., [62], supersaturation *S* can be defined as follows:

$$S = \frac{C_{Mg^{2+}} \cdot C_{OH^-}^2 - K_{eq}}{K_{eq}}$$

(16)

where C_i is the molar concentration of the *i*-th ion and K_{eq} is the equilibrium constant for the formation of $Mg(OH)_2$ which, at T=298 K, is $K_{eq} = 5.61 \times 10^{-12}$, as reported by the aforementioned authors. The induction time t_{ind}, namely the time between the onset of supersaturation and the formation of a new solid phase, depends on *S* according to the following expression:

$$\ln(t_{ind}) = A + B \cdot \left(\frac{1}{\ln S}\right)^2$$

(17)

The coefficients *A* and *B* for Eq. (1) at T= 298 K can be obtained by regression from the experimental work of Yuan *et al*. [62], thus allowing one to estimate the induction time at a temperature slightly higher than that typical of the present experiments (T=293 K). The obtained values are as follows:

t_{ind} (C_{Mg} = 0.1 mol·L^{-1} ; C_{OH^-} = 0.2 mol·L^{-1}) = 0.081 s; t_{ind} (C_{Mg} = 0.2 ; C_{OH^-} = 0.4) = 0.073 s.

Taking into account that *B* is a decreasing function of *T*, these values represent an underestimate of t_{ind} at T=293 K.

Remembering that the residence time τ_2 = 0.103 s in the tube downstream the mixers is $\tau_2 > t_{ind}$ at all concentration values here adopted, one can conclude that the fluid dynamic conditions allow the necessary

time for the kinetics of NP synthesis form primary particles, whose characterisation is described in the following chapter.

Table 2 Calculated values for *Kn*, *Stk* and *Pe* according to the variability range of diameters typical of an air-blast nebulizer as the one adopted in the present study.

Dimensionless number	Particle diameter/m	
	1×10^{-5}	1×10^{-6}
Kn	1.308×10^{-2}	1.308×10^{-1}
Stk	0.438	5.02×10^{-3}
Pe	1.413×10^{10}	1.23×10^{9}

3.3. NPs characterisation

In Fig. 7, the distribution functions of particle diameters by number have been reported for Y-shaped and T-shaped mixers and for two different concentrations of precursors, namely 0.1/0.2 mol·L^{-1} and 0.2/0.4 mol·L^{-1} for $MgSO_4$/NaOH, respectively. The average NPs diameters are in a range of 29–62 nm, while the peak values belong to a range of 27–58 nm. The relevant statistical data pertaining to each case have been reported in Table 3.

The influence of a mixer-reactor angle, which is almost negligible at low concentrations of precursors, becomes appreciable at higher concentration of reagents. As expected, whatever the type of mixer, a higher concentration of precursors tends to increase, though moderately, the average NPs diameters. An analogous result has been generally observed in NPs synthesis carried out by wet chemical bottom-up processes. In this context, Choi and Tae [63] synthesized Pt NPs in mixed solvents by photoreduction of a Pt precursor by means of ultraviolet irradiation using Pt salts at various concentrations. As in the present study, the NPs so prepared had diameters growing for increasing concentration of the precursor. These results are not only limited to NPs made of zerovalent metals, but they have been likewise reported in other investigations pertaining to the synthesis of nanostructured inorganic compounds used in optoelectronics, theranostics and catalysis. Examples can be found in many experimental studies concerning the formation of oxide- [64] and sulfide-based NPs [65]. Similarly, Malinowska *et al.* [66] observed an increase of $CoFe_2O_4$ NPs diameters for growing concentration of the metallic precursor.

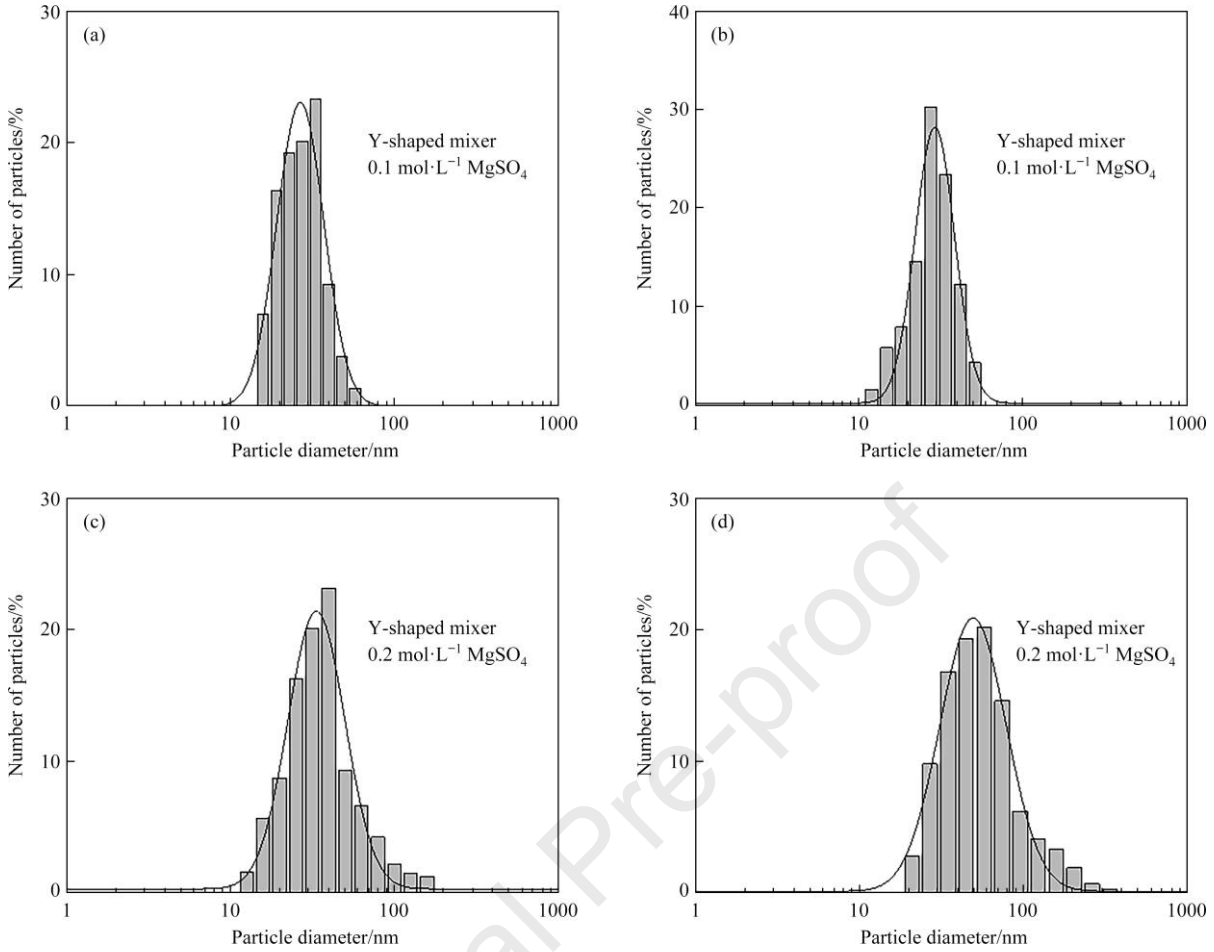

Fig. 7. Plots of particle diameter distribution functions by number for $MgSO_4$/NaOH concentrations of 0.1/0.2 mol·L^{-1} (panels a,b) and 0.2/0.4 mol·L^{-1} (panels c,d). Solid curves are lognormal interpolation plots.

Table 3 Statistical properties of $Mg(OH)_2$ NPs diameters according to the distribution curves depicted in Fig. 7.

Precursor concentration, $MgSO_4$/NaOH/mol·L^{-1}	Mixer configuration	Average NP diameter/nm	Peak value
0.1/0.2	Y-shaped	29.8	33.1
0.1/0.2	T-shaped	31.5	27.5
0.2/0.4	Y-shaped	39.3	39.8
0.2/0.4	T-shaped	61.2	57.5

In Fig. 8, single and agglomerated $Mg(OH)_2$ NPs are visible at 500'000 X magnification. The measured diameters of the relevant primary particles, taken as samples in the visual field, are in the range 17–41 nm and 31–71 nm for $MgSO_4$/NaOH precursor concentration of 0.1/0.2 and 0.2/0.4 mol·L^{-1}, respectively. These results are fully consistent with the findings obtained by DLS statistical data.

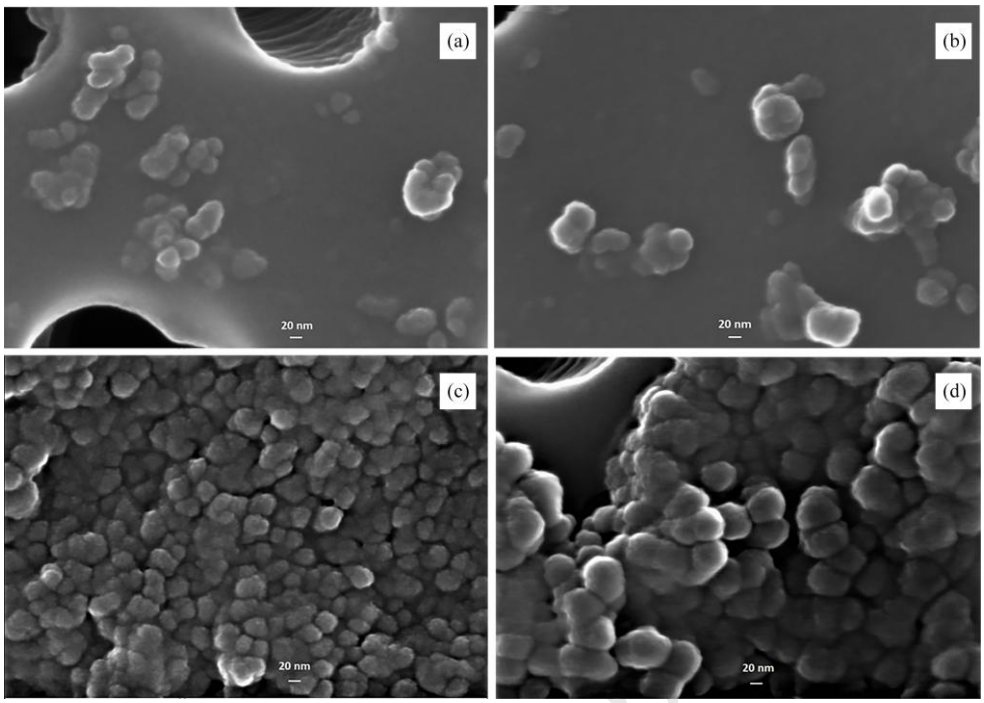

Fig. 8. FESEM images of a $Mg(OH)_2$ NPs obtained with a $MgSO_4$/NaOH concentration of 0.1/0.2 mol·L^{-1} (panels a,b) and 0.2/0.4 mol·L^{-1} (panels c,d). Panels (a) and (c) refer to a Y-shaped mixer, while panels (b) and (d) refer to a T-shaped mixer.

An X-EDS microanalysis of the nanosized solid synthesized according to the experimental conditions of Fig. 8(d) has been carried out to ascertain the presence of $Mg(OH)_2$ in the NPs. The results are visible in Fig. 9. The oxygen peak does not match the stoichiometry of $Mg(OH)_2$ composition owing to the interference of the polymeric substrate, whose oxygen content overlaps to the fraction contained in $Mg(OH)_2$.

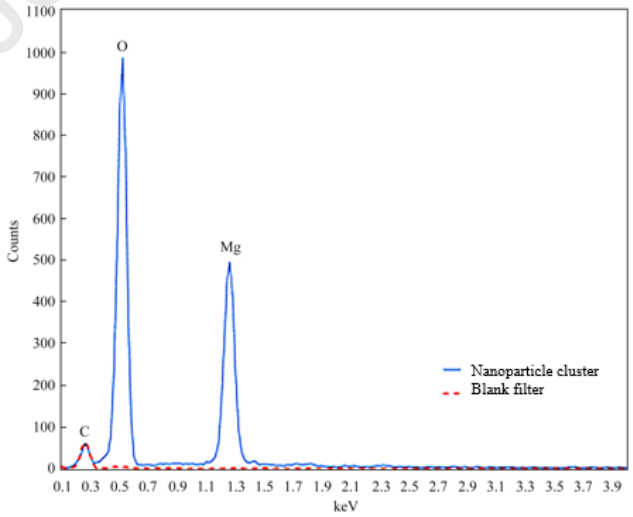

Fig. 9. X-ray compositional spectrum of $Mg(OH)_2$ NPs.

In Fig. 10, the XRPD plot of the synthesized $Mg(OH)_2$ NPs has been reported for $MgSO_4$/NaOH concentrations of 0.1/0.2 mol·L^{-1}, using a Y-shape mixer. The trend is consistent with a high purity product, as no significant spurious peak has been detected.

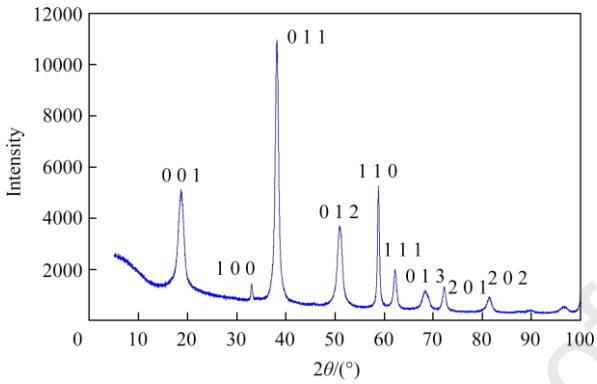

Fig. 10. XRPD spectrum of $Mg(OH)_2$ NPs.

Finally, looking ahead to a future scale-up of the plant, one can draw some considerations regarding the total energy dissipated for the synthesis of the final product according to the following data.

- Experimentally, the power required for the operation of the two pneumatic nebulisers at a minimum inlet pressure of 40 kPa is approximately equal to 12 W, adopting a membrane air compressor. The power required by the peristaltic pump to operate the four nozzles of the spray tower was measured at approximately 30 W.
- The average energy demand for anhydrous $MgSO_4$ and NaOH production have been estimated at 54 and 5.7 MJ·kg^{-1}, respectively, using literature data [67].
- The reagent mass loss in pipes and condense separators has been limited to a range of 15%–30% of the total nebulized mass. This result has been obtained by minimizing the pipe lengths downstream the nebulisers. This result represents a step forward compared to a previous study based on the use of ultrasonic atomisers [29].
- Considering the reagent flow rate reported in Fig. 5, assuming a concentration of 0.2/0.4 mol·L^{-1} for $MgSO_4$/NaOH precursors from the data of Table 3, one can deduce a final $Mg(OH)_2$ NPs energy processing cost in the range 4090–4965 MJ·kg^{-1}. These values are higher than required for producing $CaCO_3$ NPs by ultrasonic nebulisation [29], but they are lower than required for TiO_2 synthesis methods by thermal plasma or flame spray pyrolysis [68]. In the present case, the energy costs of the reagents are almost negligible compared to the processing energy costs.

4. Conclusions

An experimental study where inorganic nanoparticles are synthesized by chemical reaction mediated by coalescence of droplets containing precursors dispersed in two different aerosolized phases is proposed. The most important results can be summarized in the following points:

- A solid nanostructured phase is obtained with a simple apparatus where a chemical reaction between precursors occurs spontaneously at room temperature, namely without the need for external energy contributions of electric, mechanic of thermal origin. The only energy contributions stem from the power required by pneumatic nebulization and by the recirculation of the liquid collecting the NPs. For these reasons, the process meets the paradigms of sustainability, energy saving and environmental soundness. Namely, the ISD principles of substitution, attenuation and simplification are fulfilled with respect to the use of friendly reagents, mild operative conditions and in series NPs collection by cyclone spray tower, preventing the release of nanomaterials into the environment and the connected environmental and health exposure risk.
- The here presented technique can be advantageously extended to the production of nanosized powders of thermolabile organic or inorganic compounds, strictly requiring low operating temperatures during the synthesis process. For this reason, this method may have promising uses in pharmaceutical industry or in fine nanochemicals manufacturing. Additionally, the final product has been obtained in pure form, namely without the need for a capping agent or surfactant that, for some end-uses, represents an unwanted by-product in the as-produced NPs.
- Except for the atomizers, currently requiring some structural adjustments, the rest of the units may operate in a continuous mode, with undoubted advantages in view of a process upsizing.
- The process architecture allows a satisfactory level of safety for the operators, which are adequately protected against accidental NPs releases in the atmosphere and in the environment.

In perspective, future development and improvement of the outlined process will focus on the use of different techniques for precursor atomization, with a view to minimizing the air flow requested by the plant with a consequent reduction of the scrubber volume for better and safer management of the unit operations downstream the reaction zone, according to the intensification guideword of inherent safety.

References

[1] W.J. Yan, P.H. Sun, C. Luo, X.F. Xia, Z.F. Liu, Y.M. Zhao, S.X. Zhang, L. Sun, F. Du, PtCo-based nanocatalyst for oxygen reduction reaction: Recent highlights on synthesis strategy and catalytic mechanism, *Chin. J. Chem. Eng*. 53 (2023) 101–123.

[2] S. Razzaque, M.D. Khan, M. Aamir, M. Sohail, S. Bhoyate, R.K. Gupta, M. Sher, J. Akhtar, N. Revaprasadu, Selective synthesis of bismuth or bismuth selenide nanosheets from a metal organic precursor: investigation of their catalytic performance for water splitting, *Inorg. Chem*. 60 (3) (2021) 1449–1461.

[3] M. Shoaib, A. Naz, F.A. Osra, S.H. Abro, S.U. Qazi, F.A. Siddiqui, M.R. Shah, A.Z. Mirza, Green synthesis and characterization of silver-entecavir nanoparticles with stability determination, *Arab. J. Chem.* 14 (3) (2021) 102974.

[4] A.P. Reverberi, M. Vocciante, E. Lunghi, L. Pietrelli, B. Fabiano, New trends in the synthesis of nanoparticles by green methods, *Chem. Eng. Trans*. 61 (2017) 667–672.
[5] N.S. Zakharov, A.N. Popova, Y.A. Zakharov, V.M. Pugachev, Synthesis of nanostructured FePt systems, *J. Phys. Conf. Ser*. 1749 (1) (2021) 012012.
[6] X.H. Ge, L.J. Mo, A.H. Yu, C.Z. Tian, X.D. Wang, C. Yang, T. Qiu, Stimuli-responsive emulsions: Recent advances and potential applications, *Chin. J. Chem. Eng*. 41 (2022) 193–209.
[7] M.L. Arsene, I. Răut, M. Călin, M.L. Jecu, M. Doni, A.M. Gurban, Versatility of reverse micelles: from biomimetic models to nano (bio)sensor design, *Processes* 9 (2) (2021) 345.
[8] T. Jasrotia, S. Chaudhary, A. Kaushik, R. Kumar, G.R. Chaudhary, Green chemistry-assisted synthesis of biocompatible Ag, Cu, and Fe_2O_3 nanoparticles, *Mater. Today Chem*. 15 (2020) 100214.
[9] K.B. Tan, D.H. Sun, J.L. Huang, T. Odoom-Wubah, Q.B. Li, State of arts on the bio-synthesis of noble metal nanoparticles and their biological application, *Chin. J. Chem. Eng*. 30 (2021) 272–290.
[10] R.J. Khan, C.Y. Lau, M.U. Farid, M.K. Islam, A.K. An, J. Yi, S.Y. Leu, Woody biomass derived nano lignin-enabled membrane with high structural stability for efficient wastewater treatment, *Process. Saf. Environ. Prot*. 182 (2024) 595–607.
[11] J. Ju, X.J. Duan, B. Sarkodie, Y.J. Hu, H. Jiang, C.Z. Li, Numerical simulation of flow field and residence time of nanoparticles in a 1000-ton industrial multi-jet combustion reactor, *Chin. J. Chem. Eng*. 51 (2022) 86–99.
[12] H.K. Kammler, L. Mädler, S.E. Pratsinis, Flame synthesis of nanoparticles, *Chem. Eng. Technol*. 24 (6) (2001) 583–596.
[13] W.Y. Teoh, R. Amal, L. Mädler, Flame spray pyrolysis: an enabling technology for nanoparticles design and fabrication, *Nanoscale* 2 (8) (2010) 1324–1347.
[14] R. Koirala, S.E. Pratsinis, A. Baiker, Synthesis of catalytic materials in flames: opportunities and challenges, *Chem. Soc. Rev*. 45 (11) (2016) 3053–3068.
[15] M. Olivas-Martinez, H.Y. Sohn, H.D. Jang, K.I. Rhee, Computational fluid dynamic modeling of the flame spray pyrolysis process for silica nanopowder synthesis, *J. Nanopart. Res*. 17 (7) (2015) 324.
[16] Y. Sung, V. Raman, H. Koo, M. Mehta, R.O. Fox, Large-eddy simulation modeling of turbulent flame synthesis of titania nanoparticles using a bivariate particle description, *AIChE. J*. 60 (2) (2014) 459–472.
[17] M. Høj, D.K. Pham, M. Brorson, L. Mädler, A.D. Jensen, J.D. Grunwaldt, Two-nozzle flame spray pyrolysis (FSP) synthesis of $CoMo/Al_2O_3$ hydrotreating catalysts, *Catal. Lett*. 143 (5) (2013) 386–394.
[18] J. Sukunta, A. Wisitsoraat, A. Tuantranont, K. Jaruwongrungsee, S. Phanichphant, C. Liewhiran, Mechanistic roles of substitutional Fe dopants on catalytic acetylene-sensing process of flame-made SnO_2 nanoparticles, *Arab. J. Chem*. 13 (1) (2020) 3043–3059.
[19] B. Buesser, S.E. Pratsinis, Design of nanomaterial synthesis by aerosol processes, *Annu. Rev. Chem. Biomol. Eng*. 3 (2012) 103–127.
[20] E. Bain Wasmund, S. Saberi, K.S. Coley, Modeling of an aerosol reactor for optimizing product properties, *AIChE. J*. 53 (6) (2007) 1429–1440.

[21] Z.D. Guo, G. Xiong, L.P. Liu, P. Li, L. Hao, Y.Y. Cao, F.P. Tian, Aerosol-assisted synthesis of hierarchical porous titanosilicate molecular sieve as catalysts for cyclohexene epoxidation, *J. Porous Mater.* 23 (2) (2016) 407–413.

[22] N. Radacsi, A.E.D.M. van der Heijden, A.I. Stankiewicz, J.H. ter Horst, Cold plasma synthesis of high quality organic nanoparticles at atmospheric pressure, *J. Nanopart. Res.* 15 (2) (2013) 1445.

[23] A. Jaworek, A.T. Sobczyk, Electrospraying route to nanotechnology: an overview, *J. Electrost.* 66 (3–4) (2008) 197–219.

[24] K. Soliwoda, M. Rosowski, E. Tomaszewska, B. Tkacz-Szczesna, G. Celichowski, M. Psarski, J. Grobelny, Synthesis of monodisperse gold nanoparticles *via* electrospray-assisted chemical reduction method in cyclohexane, *Colloids Surf. A Physicochem. Eng. Aspects* 482 (2015) 148–153.

[25] P.R. Amyotte, F.I. Khan, The role of inherently safer design in process safety, *Can. J. Chem. Eng.* 99 (4) (2021) 853–871.

[26] A. Bassani, C. Vianello, P. Mocellin, A. Dell'Angelo, G. Spigno, B. Fabiano, G. Maschio, F. Manenti, Aprioristic integration of process operations and risk analysis: definition of the weighted F&EI-based concept and application to AG2S technology, *Ind. Eng. Chem. Res.* 62 (1) (2023) 500–510.

[27] B. Fabiano, A.P. Reverberi, P.S. Varbanov, Safety opportunities for the synthesis of metal nanoparticles and short-cut approach to workplace risk evaluation, *J. Clean. Prod.* 209 (2019) 297–308.

[28] A.P. Dicks, A. Hent, Green chemistry and associated metrics, In: *Green Chemistry Metrics*, Springer International Publishing, New York, 1–15 (2014).

[29] B. Fabiano, M. Salerno, M. Vocciante, O. Soda, A.P. Reverberi, A double closed-loop process for nanoparticle synthesis *via* aerosol mixing and venturi jet scrubbing, *Appl. Sci.* 15 (14) (2025) 7693.

[30] H.Y. Shen, Y.Z. Liu, One-step synthesis of hydrophobic magnesium hydroxide nanoparticles and their application in flame-retardant polypropylene composites, *Chin. J. Chem. Eng.* 26 (10) (2018) 2199–2205.

[31] C. Henrist, J.P. Mathieu, C. Vogels, A. Rulmont, R. Cloots, Morphological study of magnesium hydroxide nanoparticles precipitated in dilute aqueous solution, *J. Cryst. Growth* 249 (1–2) (2003) 321–330.

[32] E. Piperopoulos, E. Mastronardo, M. Fazio, M. Lanza, S. Galvagno, C. Milone, Enhancing the volumetric heat storage capacity of $Mg(OH)_2$ by the addition of a cationic surfactant during its synthesis, *Appl. Energy* 215 (2018) 512–522.

[33] P.M. Sy, N. Anton, Y. Idoux-Gillet, S.M. Dieng, N. Messaddeq, S. Ennahar, M. Diarra, T.F. Vandamme, Pickering nano-emulsion as a nanocarrier for pH-triggered drug release, *Int. J. Pharm.* 549 (1–2) (2018) 299–305.

[34] W. Guo, W.L. Bu, Y.F. Mao, E.Y. Wang, Y.J. Yang, C. Liu, F. Guo, H.M. Mai, H. You, Y. Long, Magnesium hydroxide as a versatile nanofiller for 3D-printed PLA bone scaffolds, *Polymers* 16 (2) (2024) 198.

[35] Z.X. Qiu, B.C. Wang, X.F. Zhou, S.Y. Yang, Q.Z. Gao, X. Cai, S.S. Zhang, Y.P. Fang, $CdS@Mg(OH)_2$ core/shell composite photocatalyst for efficient visible-light photocatalytic overall water splitting, *Int. J. Hydrog. Energy* 47 (14) (2022) 8729–8738.

[36] A.P. Reverberi, P.S. Varbanov, M. Vocciante, B. Fabiano, Bismuth oxide-related photocatalysts in green nanotechnology: a critical analysis, *Front. Chem. Sci. Eng.* 12 (4) (2018) 878–892.
[37] C.A. Uko, J.O. Tijani, S.A. Abdulkareem, S. Mustapha, T.C. Egbosiuba, E. Muzenda, Adsorptive properties of MgO/WO_3 nanoadsorbent for selected heavy metals removal from indigenous dyeing wastewater, *Process. Saf. Environ. Prot.* 162 (2022) 775–794.
[38] C.X. Ding, Z. Jin, Q.X. Li, S.H. Zhou, Y.R. Sun, Effective removal of fluoride from wastewater by magnesium oxide-loaded aeolian sand with high loading ratio, *Chin. J. Chem. Eng.* 87 (2025) 369–380.
[39] A. Fan, H.J. Gao, Synthesis of MgO nanostructures through simple hydrogen peroxide treatment for carbon capture, *Process. Saf. Environ. Prot.* 156 (2021) 361–372.
[40] Z. Fattah, M. Rezaei, A. Biabani-Ravandi, A. Irankhah, Preparation of Co–MgO mixed oxide nanocatalysts for low temperature CO oxidation: Optimization of preparation conditions, *Process. Saf. Environ. Prot.* 92 (6) (2014) 948–956.
[41] G. Balducci, L. Bravo Diaz, D.H. Gregory, Recent progress in the synthesis of nanostructured magnesium hydroxide, *CrystEngComm* 19 (41) (2017) 6067–6084.
[42] A. Clemente, M.P. Lobera, F. Balas, J. Santamaria, A versatile generator of nanoparticle aerosols. A novel tool in environmental and occupational exposure assessment, *Sci. Total Environ.* 625 (2018) 978–986.
[43] Y. Li, Y.L. Hou, H. Suo, F. Liu, S.W. Zhang, D.X. Zeng, The effect of supply gas pressure on the atomization characteristics of medical air-compression nebulizers, *ACS Omega* 10 (21) (2025) 22099–22111.
[44] A. Ramesh Kumar, G. Hota, A. Mehra, K.C. Khilar, Modeling of nanoparticles formation by mixing of two reactive microemulsions, *AIChE. J.* 50 (7) (2004) 1556–1567.
[45] E. Vafa, M. Shahrokhi, A. Molaei Dehkordi, Population balance modeling of barium sulfate nanoparticle synthesis *via* inverse microemulsion including coagulation effect, *Ind. Eng. Chem. Res.* 53 (32) (2014) 12705–12719.
[46] A. Bahmanyar, G. Pazuki, M. Nikazar, Online monitoring and mass transfer modelling of the growth of Ni-B nanoparticles in a reverse micelle system, *Can. J. Chem. Eng.* 97 (S1) (2019) 1440–1450.
[47] Y.C. Li, C.W. Park, Particle size distribution in the synthesis of nanoparticles using microemulsions, *Langmuir* 15 (4) (1999) 952–956.
[48] R. Bandyopadhyaya, R. Kumar, K.S. Gandhi, Simulation of precipitation reactions in reverse micelles, *Langmuir* 16 (18) (2000) 7139–7149.
[49] G.V. Mudzhikova, E.N. Brodskaya, Computer simulation of reverse micelles and water-in-oil microemulsions, *Colloid J.* 74 (3) (2012) 269–279.
[50] H. Samareh Fekri, M. Ranjbar, A. Pardakhty, A systematic study of Cu nanospheres embedded in non-ionic surfactant-based vesicle: photocatalytic efficiency and *in vivo* imaging study, *J. Clust. Sci.* 30 (3) (2019) 561–570.
[51] D. Dodoo-Arhin, M. Leoni, P. Scardi, E. Garnier, A. Mittiga, Synthesis, characterisation and stability of Cu_2O nanoparticles produced *via* reverse micelles microemulsion, *Mater. Chem. Phys.* 122 (2–3) (2010) 602–608.

[52] L.B. Liu, N. Xiang, Z.H. Ni, Droplet-based microreactor for the production of micro/nano-materials, *Electrophoresis* 41 (10–11) (2020) 833–851.

[53] I. Khan, K. Saeed, I. Khan, Nanoparticles: properties, applications and toxicities, *Arab. J. Chem.* 12 (7) (2019) 908–931.

[54] B.T. Chen, R.A. Fletcher, Y.-S. Cheng, Calibration of aerosol instruments, In: Aerosol Measurement: Principles, Techniques, and Applications, P. Kulkarni, P.A. Baron, K. Willeke (Eds.), John Wiley and Sons, New York (2011).

[55] S.G. Jennings, The mean free path in air, *J. Aerosol Sci.* 19 (2) (1988) 159–166.

[56] S.R. Wilson, Y. Liu, E.A. Matida, M.R. Johnson, Aerosol deposition measurements as a function of Reynolds number for turbulent flow in a ninety-degree pipe bend, *Aerosol Sci. Technol.* 45 (3) (2011) 364–375.

[57] M. Heim, R. Wengeler, H. Nirschl, G. Kasper, Particle deposition from aerosol flow inside a T-shaped micro-mixer, *J. Micromech. Microeng.* 16 (1) (2006) 70–76.

[58] C.N. Davies, Coagulation of aerosols by Brownian motion, *J. Aerosol Sci.* 10 (2) (1979) 151–161.

[59] J. Geng, H. Park, E. Sajo, Simulation of aerosol coagulation and deposition under multiple flow regimes with arbitrary computational precision, *Aerosol Sci. Technol.* 47 (5) (2013) 530–542.

[60] A. Chatterjee, M. Kerker, D.D. Cooke, Brownian coagulation of aerosols in the transition regime, *J. Colloid Interface Sci.* 53 (1) (1975) 71–82.

[61] A. Raponi, S. Romano, G. Battaglia, A. Buffo, M. Vanni, A. Cipollina, D. Marchisio, Computational modeling of magnesium hydroxide precipitation and kinetics parameters identification, *Cryst. Growth Des.* 23 (7) (2023) 4748–4759.

[62] Q.H. Yuan, Z.W. Lu, P.X. Zhang, X.B. Luo, X.Z. Ren, T.D. Golden, Study of the synthesis and crystallization kinetics of magnesium hydroxide, *Mater. Chem. Phys.* 162 (2015) 734–742.

[63] S.W. Choi, Y.T. Byun, The effect of platinum precursor concentrations on chlorine sensing characteristics of platinum nanoparticles−loaded single walled carbon nanotubes, *Appl. Surf. Sci.* 433 (2018) 480–486.

[64] X.K. Zhang, Y.C. Rui, Y.Q. Wang, J.L. Xu, H.Z. Wang, Q.H. Zhang, P. Müller-Buschbaum, SnO_2 nanorod arrays with tailored area density as efficient electron transport layers for perovskite solar cells, *J. Power Sources* 402 (2018) 460–467.

[65] S. Thakur, R. Kaur, S.K. Mandal, Size dependence of CdS nanoparticles on the precursor concentration and visible light driven photocatalytic degradation of methylene blue, *New J. Chem.* 45 (27) (2021) 12227–12235.

[66] I. Malinowska, Z. Ryżyńska, E. Mrotek, T. Klimczuk, A. Zielińska-Jurek, Synthesis of $CoFe_2O_4$ nanoparticles: the effect of ionic strength, concentration, and precursor type on morphology and magnetic properties, *J. Nanomater.* 2020 (1) (2020) 9046219.

[67] A. Kumar, F.M. Du, J.H.V. Lienhard, Caustic soda production, energy efficiency, and electrolyzers, *ACS Energy Lett.* 6 (10) (2021) 3563–3566.

[68] F. Wu, Z. Zhou, A.L. Hicks, Life cycle impact of titanium dioxide nanoparticle synthesis through physical, chemical, and biological routes, *Environ*. *Sci*. *Technol*. 53 (8) (2019) 4078–4087.

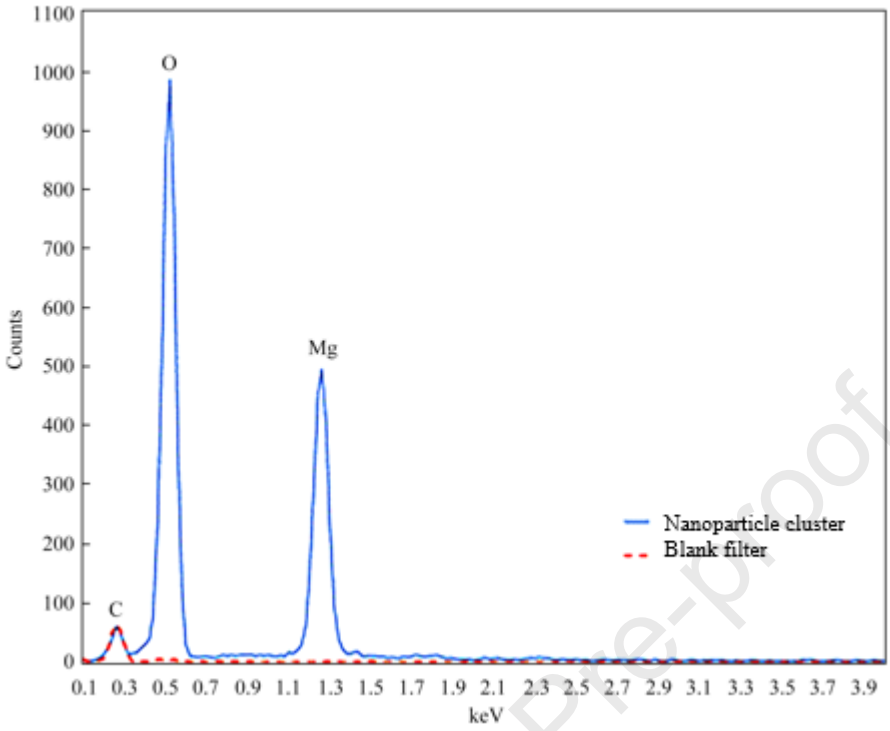

Declaration of Interest Statement

☒ The authors declare that they have no known competing financial interests or personal relationships that could have appeared to influence the work reported in this paper.

☐ The author is an Editorial Board Member/Editor-in-Chief/Associate Editor/Guest Editor for this journal and was not involved in the editorial review or the decision to publish this article.

☐ The authors declare the following financial interests/personal relationships which may be considered as potential competing interests: